Journal of Colloid and Interface Science 426 (2014) 9–21

Contents lists available at ScienceDirect

Journal of Colloid and Interface Science

www.elsevier.com/locate/jcis

Factors controlling the formation and stability of foams used as precursors of porous materials

I. Lesov, S. Tcholakova *, N. Denkov

Department of Chemical Engineering, Faculty of Chemistry and Pharmacy, Sofia University, 1 James Bourchier Ave., 1164 Sofia, Bulgaria

ARTICLE INFO

Article history:
Received 11 November 2013
Accepted 28 March 2014
Available online 3 April 2014

Keywords:
Foamability
Foam stability
Foam rheology
Suspension rheology
Particle stabilized foams
Porous materials
Solid foams

ABSTRACT

The remarkable stability of particle-stabilized foams and the opportunity to use them for production of novel porous materials have been attracting the researchers' attention in the recent years. The major aim of the current study is to clarify the factors, controlling the foamability and stability of foams, formed from concentrated silica suspensions in the presence of the amphoteric surfactant CAPB. The experiments showed that: (1) two regions can be defined with respect to suspension foaminess: Region 1 – good foaming and Region 2 – strongly suppressed foaming. The foam volume decreased linearly with the increase of suspension viscosity, so that Region 2 appears as a result of the excessively high suspension viscosity. (2) Based on foam stability four sub-regions were observed in Region 1: region 1S – stable foams, which can be dried to form stable porous materials; 1UD – foams which are unstable with respect to water drainage and collapse upon drying; 1UC – foams which are stable to drainage, but are unstable to drying, due to crack formation; 1UF – unstable foams which completely fall apart upon drying. (3) Foams in Regions 1S and 1UC had yield stress above 10 Pa which prevented liquid drainage, while foams from Region 1UD drained because of their lower yield stress. (4) The particles in the foams assembled in a 3D network in the Plateau channels and the nodes, while surfactant stabilized the foam films between the bubbles. These results define the conditions, appropriate for formation of stable, highly porous silica materials with low mass density, which can be further modified (sintered, impregnated, hydrophobized, etc.) to serve as catalyst supports, porous filters, insulating materials, etc.

1. Introduction

Particle-stabilized foams [1–26] and emulsions [25–36] have attracted considerable research interest recently, due to their unique properties and potential technological applications. Among the most interesting applications are those related to the possibility for fabrication of porous materials with complex hierarchical structure, by using particle-stabilized drops or bubbles as templates [18–28]. Several groups described procedures for generation and stabilization of foams by appropriate particle–surfactant mixtures [1–17]. In some of these studies it was shown that inorganic colloidal particles can be hydrophobized in situ, by adsorption of short-chain amphiphilic molecules, and these surface-modified particles can act as very efficient foam stabilizers [2,3,9,10,14,23]. The effect of the composition of the initial colloidal suspension on the air volume fraction, average bubble size, and bubble size distribution in the formed wet foams was investigated [23]. In other studies, [12–14,16] aqueous foams prepared by dispersions of disk-shaped Laponite particle and containing the cationic surfactant cetyltrimethylammonium bromide (CTAB), were studied. All these studies showed that the foams could be stabilized by two basic, qualitatively different mechanisms: (a) adsorption of surfactant-modified particles on the bubble surface and the related stabilization of the foam films by the particles; (b) formation of a network by aggregated particles in the foaming phase [12,17].

The particle modification by adsorbing surfactant molecules is highly specific and depends on the type and concentration of surfactants and particles [2,10,12,15,16]. Therefore, it is still very difficult (or impossible) to predict what would be the foamability of such particle–surfactant mixtures and what would be the stability of the generated foams. For example, Sepulveda and Binner [19] claimed that suspension viscosity had a little effect on the final volume of the generated foam, whereas Dhara and Bhargava [22] observed that the total porosity of the final material decreased linearly with the increase of suspension viscosity. Thus we see that even the "simple" effect of suspension viscosity, which is governed

* Corresponding author. Fax: +359 2 962 5643.
E-mail address: SC@LCPE.UNI-SOFIA.BG (S. Tcholakova).

http://dx.doi.org/10.1016/j.jcis.2014.03.067
0021-9797/

by the surfactant–particle interactions, is under discussion and might be system dependent.

The major aims of the current study are: (1) to reveal the mechanisms of foam stabilization for concentrated silica dispersions, containing the zwitterionic surfactant cocoamidopropyl betaine, CAPB; (2) to determine the main physico-chemical factors which control the foamability and foam stability with respect to liquid drainage, bubble coarsening, bubble coalescence and foam drying for the foamed CAPB-silica suspensions.

CAPB surfactant was chosen for this study because, as shown in Section 3.6 below, it leads to formation of foams with foam films stabilized by surfactant molecules (not by particles). Accordingly, the final porous structure is with open cells – these foam films break in the process of drying, thus opening direct access between the neighboring bubbles. From this viewpoint, CAPB differs from most of the surfactants used in this area which provide particle-stabilized foam films, thus leading (usually) to closed cells in the final porous material.

To achieve these aims, we performed foaming experiments under well-defined conditions, combined with a set of complementary model experiments. Namely, the rheological properties of CAPB-silica dispersions were characterized to clarify their relation to the foamability of the dispersions and to the stability of the generated foams. Optical observations of the foam films and of the real foams were performed to clarify the mechanism of foam stabilization (by particles or by adsorbed surfactant molecules). Foam stability during long-term shelf storage and upon drying was monitored. Whenever possible, quantitative expressions are proposed to describe the relations between suspension and foam properties.

The focus of the current study is mainly on the formation and stability of the wet foam precursors. The subsequent process of foam drying to produce the final porous material (and the related changes in the foam structure during drying) is investigated in detail in a separate study, see Ref. [24].

2. Materials and methods

2.1. Materials

We used amorphous precipitated silica particles (Tixosil 365, Rhodia) with silica concentration in the batch powder $\geqslant$87.5 wt%. The commercial silica powder contains also 1.5 wt% soluble salts, and 11% physically and chemically bound water. According to the producer, specific surface area of the silica particles is 150 ± 10 m^2/g, mean agglomerate diameter is $d_{50} \approx 3.5$ μm, and mass density of the particle material is 2100 kg/m^3.

Amphoteric surfactant cocoamidopropyl betaine (CAPB) was used as additive for foam stabilization. Commercial product Tego Betain F50 from Goldschmidt GmbH, containing 40 wt% of active CAPB, was used. According to Tzocheva et al. [37] the commercial Tego betaine F50 contains also admixtures of 2.8 wt% non-reacted coco fatty acids and 7.3 wt% NaCl. The composition of the coco fatty acids is 5–9% octanoic acid (C_8); 6–10% decanoic acid (C_{10}), 44–52% dodecanoic acid (C_{12}), 13–19% tetradecanoic acid (C_{14}); 8–11% hexadecanoic acid (C_{16}); 1–3% octadecanoic acid (C_{18}) and 5–8% oleic acid. Respectively, the main surfactant CAPB is also a mixture of molecules with a distribution of the hydrocarbon chain lengths, reflecting the composition of the initial coco fatty acid source from which CAPB is synthesized.

Deionized water from Elix 3 module (Millipore) was used for preparation of all solutions and suspensions. Sodium chloride and sodium hydroxide from Sigma–Aldrich were used in suspension preparation, both being of analytical grade (>99.9% pure).

2.2. Suspension preparation

Initially, suspensions with 21 wt% particle concentration were prepared by mixing the necessary amounts of silica particles and deionized water. This mixture was placed on a ball mill drive (BML-2, Witeg) at 125 rpm for 30 min. Afterwards, the suspension was homogenized for 2 h with a pulse sonicator (SKL-650 W, Syclon) which was set to 1 s long pulses with power output of 650 W (followed by 0.5 s off), using a sonotrode with diameter of 10 mm. Next, portions of 2 M solution of NaOH (in proportion of 0.12 g solution per 1 g silica in the suspension) were added to adjust the pH to 8.5. Finally, this suspension was homogenized for additional 5 min at the ball mill and for 60 min at the sonicator. Dynamic light scattering measurements on diluted suspensions showed that the aggregate size has been reduced after this procedure down to the range between 50 and 300 nm.

Suspensions with lower particle concentrations were obtained by diluting the original 21 wt% suspension with the necessary amount of deionized water or CAPB solution, just before the foaming experiments. Suspensions with particle concentration above 21 wt% were prepared by stepwise addition of more silica and NaOH to the initial 21 wt% suspension, followed by homogenization for 5 min at the ball mill and for 1–2 h at the sonicator after each step. Maximum concentration of 25.7 ± 0.5 wt% silica could be obtained in this way. Further increase of particle concentration led to severe suspension gelling.

The working pH = 8.5 was chosen after an initial series of screening experiments about the effects of pH and electrolytes (NaCl and $CaCl_2$) on the foaming and foam stability. These experiments showed that best results with respect to foam stability are obtained at low electrolyte concentrations and high pH. Therefore, all systematic experiments are performed without additional electrolytes and at pH = 8.5. Higher pH was not used to avoid possible (partial) dissolution of the silica particles in the form of sodium silicate.

2.3. Foam generation and foam stability

Planetary mixer (Kenwood Chef Premier KMC 560, 1000 W) was used for foaming of the suspensions. A given mass of the suspension, m_s, was introduced in the mixer and a complementary quantity of surfactant stock solution was added, so that the total amount of suspension + surfactant solution was always 400 g. The mixer was initially set at minimum mixing speed (32 rpm) for 4 min to form a homogeneous silica-CAPB suspension without foaming. Then higher mixing speed of 165 rpm was applied for 10 min. According to the model of the flow inside this mixer, developed by Chesterton et al. [38] the mixing speed in our experiments corresponds to shear rates of $\approx 100\ s^{-1}$. Afterwards, mixing was stopped and foam samples were taken for determination of the air volume fraction and for characterization of the foam stability with respect to liquid drainage, bubble Ostwald ripening, and foam drying.

To determine the volume fraction of trapped air, Φ, we filled a petri dish with foam of known volume, V_F = 28 mL, and measured its mass, m_F. Then Φ was determined from the relation $\Phi = (1 - m_F/V_F\rho_S)$. Here, ρ_S is the mass density of the silica suspension, calculated assuming ideal mixing of particles with mass density 2100 kg/m^3 (as provided by the producer) and water (997 kg/m^3).

To determine foam stability with respect to liquid drainage, a foam sample was transferred in a petri dish of 100 mL with height of 3.5 cm, and observed for several days to check whether aqueous phase is collected at the bottom of the container, as a result of drainage. Similar sample was used to monitor the stability of the foams with respect to bubble collapse and bubble Ostwald

ripening. To evaluate the rate of Ostwald ripening, we observed the changes in the size of the bubbles in the uppermost layer of the foam, within the first 1–2 h after foam generation. This observation was conducted in reflected light with optical microscope Axioplan (Zeiss, Germany), equipped with a long-distance objective Zeiss Epiplan 20×/0.40, CCD camera, video-recorder and monitor.

The foam stability upon drying was determined with 50–70 ml foam samples, placed in a petri dish (3.5 cm high × 6 cm diameter). The foam samples were dried at ambient temperature (28 ± 5 °C) and humidity (30–45%). The container was covered with a filter paper, which did not touch the foam sample, to moderate the rate of water evaporation from the foam.

After foam drying, we observed the structure of the dried porous material by Scanning Electron Microscopy (SEM) instrument TESCAN LYRA3 GM, Czech Republic. For these observations, dried samples were broken into pieces and a small piece ($2 \times 2\ cm^2$) was taken from the middle of the sample and coated with Au/Pd alloy via low-vacuum sputter coating.

2.4. Suspension rheology

The rheological properties of the studied suspensions were characterized by Gemini rotational rheometer (Malvern Instruments, UK), at 25 °C. All experiments were performed by using parallel plate geometry, with radius of 20 mm and gap-width of 500 μm. Sandpaper (P 1500, app. 12 μm grain size) was glued on both plates of the rheometer to suppress possible wall-slip of the samples.

Suspension viscosity was determined by using the following procedure: 25 g suspension was sonicated for 5 min at maximum power output (1 s pulse and 0.5 s off). Because the suspension heats up during sonication, it was left to cool down to 30 °C for 10 min and the necessary amount of stock surfactant solution was added. The suspension containing silica particles and surfactant was homogenized manually with a spatula for 30 s, at around 150 rpm, and then placed in the rheometer. The suspension viscosity was measured as a function of time, $\eta_{app}(t)$, at constant shear rate, for a period of 2000 s. This procedure was chosen to mimic as close as possible the initial period of suspension + surfactant homogenization at low shear rate in the foaming mixer (before starting the actual foaming at higher shear of the suspension).

Afterwards, the suspension shear stress, τ, was measured as a function of the shear rate, $\dot{\gamma}$, in the interval between 100 and 2000 s^{-1}, going logarithmically from low to high rates and backwards, over a period of 50 s in each direction. The curve from high to low speeds was fit by Bingham rheological model. From the best fit we determine the yield stress, τ_0, consistency, k, and the respective effective viscosity of the suspension, $\eta_{app}(t)$.

2.5. Surface tension

The surface tension of CAPB solutions, in the presence of 40 mM NaCl at pH = 8.5, was measured by the pendant drop method on instrument DSA 10 (Krüss, Germany) at T = 25 °C. In separate series of experiments, suspensions with different concentrations of particles and CAPB were prepared by the procedure, described in Section 2.2. These suspensions were centrifuged for 40 min at 15000 rpm (Sigma Laborzentrifugen 3–16 PK, Rotor 12158) and 25 °C to separate the particles from the aqueous phase. The supernatant above the particle sediment was decanted and its surface tension was measured, as a function of time.

2.6. Zeta potential

Zeta potential of the silica particles in the presence of CAPB was measured with a Zetasizer Nano ZS instrument (Malvern, UK) at 25 °C. The centrifugation procedure for sample preparation from Section 2.5 was applied to separate the particles from the equilibrated aqueous phase. Next 0.1 g of the centrifuged sediment was re-dispersed back into the supernatant to measure the electrophoretic mobility of the silica particles. At least 3 individual samples were measured, with 100 runs per sample. Average zeta potential was then calculated and the data scattering is presented as error bars.

2.7. Foam films

Foam films of millimeter size, formed from silica-surfactant suspensions, were observed in a capillary cell to obtain information about the film stability, film-thinning pattern, and the tendency of the silica particles to stabilize the films. The observations were performed in reflected light, by using the method of Scheludko [39]. The foam film is formed from a biconcave drop, placed in a short capillary (i.d. 2.5 mm, height 3 mm), by sucking out liquid through a side orifice. The observations are performed in reflected light with microscope Axioplan (Zeiss, Germany) equipped with a long-distance objective Zeiss Epiplan 20×/0.40, CCD camera, video-recorder and monitor.

3. Experimental results

In this section we present experimental results about the surfactant adsorption on particle surface, kinetics of foam generation, foam stability, suspension yield stress and viscosity, and foam film thinning behavior. Overall discussion of all obtained results and some additional quantitative relations are presented in Section 4.

3.1. Surfactant adsorption on particle surface

In this section we quantify the amount of adsorbed surfactant on the particle surface, in order to use this information in the analysis of the data, obtained by the other experimental methods.

First, we checked whether the original silica particles contain surface active impurities. For this purpose we measured the surface tension of the supernatant of silica suspensions, without any surfactant added. These experiments showed that the surface tension remained very close to that of pure water ≈70.5 ± 1 mN/m in the first 400 s of the measurement, which shows that the concentration of surface active impurities in the particle suspensions is rather low.

Next, we determined the amount of CAPB which is adsorbed on the particle surface. For this purpose we determined by HPLC the CAPB concentrations in the aqueous phase before and after its contact with the silica particles (the exact HPLC procedure is proprietary information and could not be disclosed now). The results showed that the alkylamidobetaine components with longer chain length ($\geqslant C_{12}$) partially adsorb on the surface of the silica particles, while the betaine components with shorter chains ($<C_{12}$) stay predominantly dissolved in the aqueous phase. The concentration of the dissolved betaines was much higher than the critical micelle concentration of the studied CAPB sample (CMC ≈ 0.031 wt% ≈ 0.9 mM) in all studied cases. Results showed also that the increase of the total CAPB concentration leads to more pronounced adsorption on the silica surface – the fraction of adsorbed alkylamidobetaines increases with the total CAPB concentration. Experiments prepared with 15.8 wt% silica suspensions showed that ≈25% of the added surfactant is adsorbed at 0.125 wt% CAPB, ≈50% is adsorbed at 0.250 wt% CAPB, ≈60% is adsorbed at 0.500 wt% CAPB, and ≈70% is adsorbed at 1.42 wt% CAPB. The respective values for the silica surface coverage by the surfactant molecules at these CAPB concentrations are 13, 50, 110 and 420 $\mu g/m^2$, respectively.

Most probably, the observed unusual increase of surfactant adsorption with the CAPB concentration (above the CMC) is due to the fact that we are dealing with a complex surfactant mixture, not with a single surfactant molecular species (see Section 2.1). The increase of CAPB concentration provides more long-chain molecules, with chain-length $\geqslant C_{12}$, available for adsorption on the silica surface. On its turn, the increased adsorption of the long-chain molecules might facilitate (promote) the adsorption of the shorter-chain molecules at higher total CAPB concentration, thus explaining the observed overall increase of surfactant adsorption.

To confirm that a large fraction of the surfactant remains in the bulk solution and to check how the surface properties of the CAPB solutions are affected by their contact with the silica particles in the suspensions, we compared the surface tension of the original CAPB solutions (without contact with silica) with that of centrifuged aqueous phase (supernatant) of silica suspensions. As seen from Fig. S1, the equilibrium surface tension of the CAPB solutions with concentration varied between 0.011 and 0.5 wt% were very similar – the reason is that these solutions are around and above the critical micelle concentration of the studied CAPB sample. As expected, the kinetics of approaching this equilibrium surface tension was faster at higher CAPB concentration, see Fig. S1. When one of these solutions, 0.5 wt% CAPB, was equilibrated with 15.8 wt% of silica particles, the surface tension of the aqueous phase turned out to be different, with slower kinetics of surface tension decrease and probably higher equilibrium surface tension (not reached even after 600 s of measurement). This comparison is a further indication that a fraction of CAPB adsorbed on the silica particles in the suspension, thus modifying their surface properties.

To check how the surfactant adsorption affects the surface charge of the particles and the electrostatic interactions between them, we measured the zeta potential of silica particles before and after their contact with CAPB solution. The procedure described in Section 2.6 was used. The obtained results for the particle ζ-potential, as a function of surfactant concentration and surfactant-to-particle ratio, are presented in Fig. S2 of the Supplementary materials. The zeta-potential of the particles without added surfactant was -40 ± 1.5 mV. When CAPB of concentration below 0.5 wt% was added to 15.8 wt% silica suspension (i.e., $C_S/C_P \leqslant 0.032$), a decrease in magnitude of the particle zeta-potential to around -30 mV was observed. Further increase in surfactant concentration up to 1.4 wt% led to a slower decrease in the zeta potential to -22 mV. These results also confirm that CAPB molecules adsorb on the particle surface.

Note that the available surfactant in the suspensions studied is insufficient to cover the silica surface with complete adsorption layer. Indeed, even if we assume that all surfactant molecules were adsorbed on the silica surface (which is not the case as explained above) the surfactant adsorption would vary between 0 and 0.69 mg/m^2 CAPB in these experiments. For comparison, a complete dense surfactant monolayer would correspond to around 2 mg/m^2 CAPB, which corresponds to about 0.3 nm^2 area per molecule in the dense adsorption layer [40]. Therefore, a loose or, most probably, patchy surfactant adsorption layers are formed on the particle surface in this range of surfactant concentrations.

The above results show clearly that fraction of the surfactant adsorbs and modifies the particles, but a significant fraction of the surfactant remains in the solution. During foaming, one could expect a competitive adsorption between the free surfactant molecules and the hydrophobized silica particles. As shown in the following sections (e.g. in Section 3.6), the surfactant turned out to be more surface active in these systems and it dominates the air–water interface, whereas the silica particles remain dispersed within the aqueous phase.

3.2. Foam generation

The kinetics of air entrapment (foam formation) was studied first with 20.6 wt% silica suspensions, at different surfactant concentrations, varied between 0 and 2.12 wt% CAPB, defined with respect to the total mass of the suspension. For the following discussion, it is convenient to describe the experimental data in terms of the dimensionless ratio of the surfactant-to-particle concentration C_S/C_P (wt/wt) which varied between zero (no surfactant) and 0.103 in these experiments, see Fig. 1A. As explained in the preceding section, the total amount of surfactant in these suspensions was insufficient to cover the silica surface by a complete surfactant monolayer. Nevertheless, we observed a significant and non-trivial effect of the surfactant on suspension foaminess even in the range of lowest surfactant concentrations studied, where the surfactant could cover less than 10% of the silica surface.

The experimental results presented in Fig. 1A show that no foam is formed while stirring a silica suspension without CAPB – the original silica particles are too hydrophilic and cannot stabilize the trapped air bubbles to form any foam. In the presence of CAPB, the kinetics of air entrapment depends strongly on both surfactant and particle concentrations, see Fig. 1A and B. At $C_p = 20.6$ wt% (see Fig. 1A), the initial increase of C_S/C_P from 1.5×10^{-4} to 0.009, corresponding to increase of C_S from 0.003 to 0.19 wt%, leads to a rapid increase of the rate of foam generation. Similar increase was observed when CAPB with comparable concentration without particles was used for foam generation (data not shown). The latter result indicates that the observed increase in suspension foaminess, in this range of low surfactant concentrations, is due primarily to the increase of surfactant concentration, not to the changed particle properties.

The further increase of C_S/C_P from 0.009 to 0.103 (corresponding to increase of C_S from 0.19 to 2.12 wt%) leads to a significant decrease in the rate of foam generation (Fig. 1A) and strongly reduced air volume fraction in the foam, generated after 600 s of suspension stirring (Fig. 1E). Under the same conditions, the foaminess of CAPB solution (without particles) is very high – foam with air volume fraction of 0.80 is formed for less than 10 s and maximum $\Phi \approx 0.96$ was reached in around 3 min. Therefore, the observed decrease in suspension foaminess at higher surfactant concentrations is related to the interactions between surfactant and particles, as explained below.

As seen from Fig. 1A, at $C_S/C_P < 0.034$, the kinetics of foam generation typically consists of two subsequent periods: in the first seconds after starting the intensive mixing of the suspension, the foam volume increases rapidly up to a given value (first period), followed by a further, much slower increase in foam volume until a plateau is reached (second period). At higher $C_S/C_P > 0.034$, we observed an initial induction period (beside the subsequent two periods, as described above), during which no significant volume of air is trapped in the sheared suspension. After certain time of shearing (ca. 100 s for $C_S/C_P = 0.051$) an almost linear increase in foam volume is observed with the time of shear, followed by plateau. This induction period is due to the high initial viscosity of the respective suspensions – see Section 3.4 and Fig. 5 for results supporting this explanation.

The effect of particle concentration on the kinetics of foam generation was studied also at fixed ratio $C_S/C_P = 0.051$, as shown in Fig. 1B. At low particle concentrations, the induction period is missing and only the two subsequent periods of fast and slow increase of foam volume are observed. The rate of air entrapment decreases with increasing particle concentration. The increase of particle concentration above 20 wt% leads to a very rapid reduction of the speed of foam generation and of the air volume fraction after 600 s of suspension stirring (Fig. 1F).

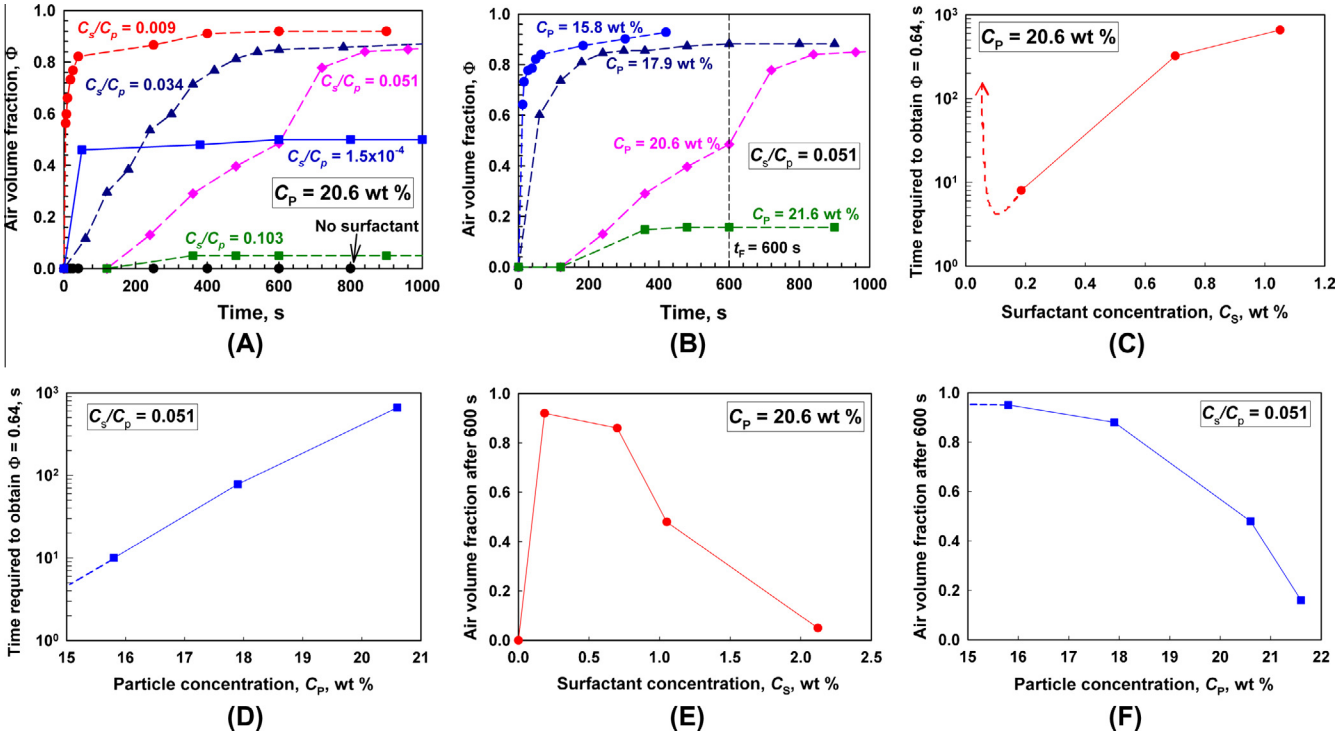

Fig. 1. Kinetics of air entrapment in a planetary mixer for silica suspensions at: (A) C_P = 20.6 wt% silica and various C_S/C_P, (B) C_S/C_P = 0.051 and different particle concentrations. Also shown are the related: (C and D) time required to obtain foam with air volume fraction of 0.64 and (E and F) air volume fraction in foams formed after 600 s of shearing, as a function of (C and E) surfactant concentration at fixed C_P = 20.6 wt%, and (D and F) particle concentration at fixed C_S/C_P = 0.051.

To quantify the rate of air entrapment in the initial (first) period, we determined the time required to obtain foam with air volume fraction of 0.64. This air volume fraction was chosen because this is the highest volume fraction at which stable porous materials could be obtained after foam drying, with the CAPB-silica suspensions studied here. To characterize the second (plateau) region, we determined the air volume fraction in the foamed suspension after 600 s of shearing. These two foam characteristics are compared in Fig. 1C–F for the various surfactant and particle concentrations studied. One sees that the time required for obtaining foam with air volume fraction $\Phi = 0.64$ increases significantly with the increase of surfactant concentration at fixed particle concentration, Fig. 1C, and with the increase of particle concentration at fixed surfactant concentration, Fig. 1D (note that only 3 of the curves in Fig. 1A or 1B reached $\Phi = 0.64$; therefore, only 3 experimental points are plotted in Fig. 1C or D). On the other hand, the air volume fraction after 600 s shearing, Φ_{600s}, passes through a high maximum, as a function of CAPB concentration and rapidly decreases with the increase of particle concentration when the latter is above 18 wt%, see Fig. 1E and F.

The obtained results from all foaming experiments could be summarized as a "foamability diagram" which includes two regions (see Fig. 2A):

(1) At C_P < 18 wt% for all studied C_S/C_P between 0.009 and 0.25, the studied suspensions showed very good foamability and foams with air volume fractions above 0.35 are formed after shearing of 600 s.
(2) At C_P > 18 wt% the increase of C_S/C_P above a certain value leads to a significant reduction of suspension foamability and the trapped air remains lower than 0.35 even after a long period of suspension shearing.

These data show that CAPB of very low concentrations, corresponding to less than 60 μg/m^2 of surface coverage only, already leads to a significant increase of Φ_{600s} from zero (no CAPB) up to 95 vol% of air. As shown in Section 3.6 below, this rapid initial increase in the foamability of the silica suspensions is due to the fact that the foam films in these samples are stabilized by the surfactant remaining dissolved in the aqueous phase, not by the silica particles themselves. However, the further increase of surfactant concentration leads to a rapid reduction of the foamability of the studied suspensions (Fig. 1C). This non-trivial result is related to the observed significant increase of suspension viscosity at higher surfactant concentrations, which is due to adsorption of some fraction of the surfactant on the particle surface, with the resulting modification of the particle–particle interactions, as explained in Section 3.4 below.

3.3. Foam stability

After foam generation, 30 ml foam was transferred into a glass bottle and covered with a cap to monitor the stability of the wet foam to liquid drainage, bubble Ostwald ripening and bubble coalescence for several months. Other 50–70 mL foam was transferred in a petri dish and the foam stability was studied in the process of its drying at room temperature.

To check how the bubble volume fraction affects the foam stability, at fixed composition of the foamed suspension, we tested first a series of foams with different air volume fractions, all formed from suspension with C_P = 15.8 wt% and C_S/C_P = 0.051. Illustrative pictures from the final output, after drying of the wet foams with different air volume fractions, are shown in Fig. 3. One sees that the foams with initial air volume fraction $\leqslant$0.65 are stable to water drainage and drying. In contrast, the foams with higher air volume fraction are unstable upon drying with respect to crack formation. As a rule, the higher initial air volume fraction leads to larger cracks in the final porous material.

Therefore, to compare the stability of foams with different compositions, we studied foams at fixed air volume fraction of 0.64.

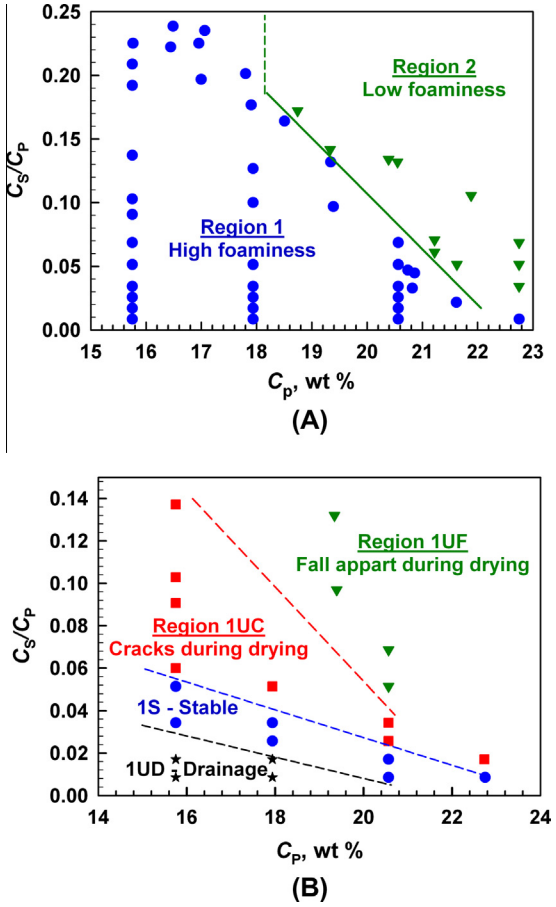

Fig. 2. (A) Foamability diagram for CAPB-silica suspensions with different particle concentrations, C_P, and surfactant-to-particle weight ratios, C_S/C_P. (B) Stability diagram for foams formed from CAPB-silica suspension with $\Phi = 0.64 \pm 0.03$.

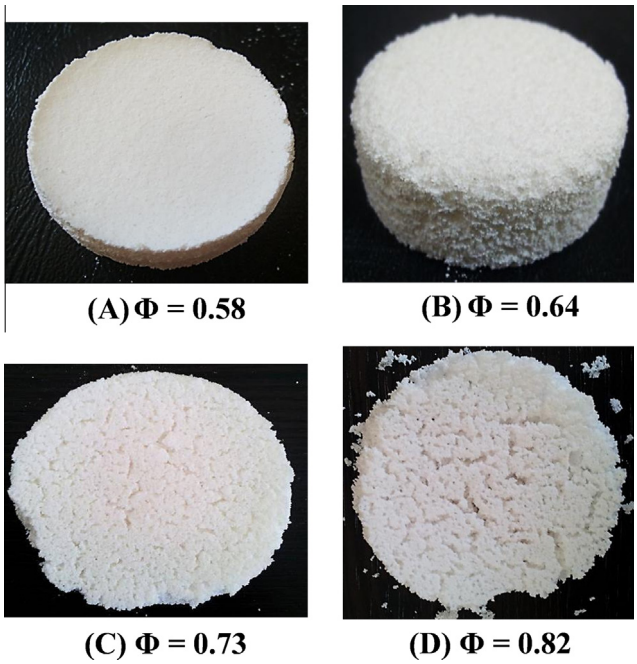

Fig. 3. Illustrative pictures of the porous materials, formed after drying of wet foams with different air volume fractions, as indicated in the figure. Wet foams are formed from CAPB-silica suspension with 15.8 wt% particles and $C_S/C_P = 0.051$.

The obtained experimental results are summarized as stability diagram in Fig. 2B which contains the following regions:

Region 1UD (UD stands for "Unstable to Drainage") – this region appears at C_S/C_P below ca. 0.02. The bubbles formed in these foams were relatively large in size, with diameter of the order of 0.5–2 mm. The bubble size further increased in the period after foam formation, and the liquid phase partially drained from the foams. As a result, the air volume fraction at the top of the foam sample increased to 85 ± 5% within 2–3 min, while suspension accumulated at the bottom of the container. As a result, these foams were unstable upon drying, due to formation of cracks which gradually increased with time, so that the final porous material was broken into pieces, see Fig. 4C.

Region 1S (S stands for "Stable") – this region appears between ca. 0.04 and 0.06 of C_S/C_P at 15 wt% silica, and between 0.01 and 0.02 of C_S/C_P at 20 wt% silica in the suspension. The foams with $\Phi = 0.64$, prepared under these conditions, were stable to liquid drainage for several months (no drainage was observed upon shelf-storage). Initially, the bubbles in these foams increased their size from *ca* 0.05 to 0.3 mm, due to Ostwald ripening. However, the suspension between the bubbles gelled with aging time, which resulted in arrest of this process. The typical period of suspension gelling depended on the concentrations of surfactant and particles, but usually developed within an hour. After gelling, the foams were completely stable to drainage and Ostwald ripening – wet foams were observed over a period of more than 18 months without any structural changes. Very small or no cracks were observed when foam samples from this region, with diameter of 6.5 cm and height between 1.5 and 3 cm, were dried at ambient conditions, see Fig. 4A. Therefore, this region was the only one appropriate for formation of stable porous materials with low final mass density (down to 100 kg/m^3). SEM images of these dried porous materials revealed that the bubble size was in the range of 200–300 μm and the pore cells were predominantly closed, see Fig. 4B. Note that the air volume fraction in these experiments, $\Phi = 0.64$, is around the close packing of spherical bubbles which means that no large foam films are formed between the neighboring bubbles in these samples.

Region 1UC (UC stands for "Unstable to Cracking") appears between 0.1 and 0.16 of C_S/C_P ratio at $C_P = 15$ wt% and between 0.03 and 0.06 at $C_P = 20$ wt%. The foams are stable to drainage in this region. Some increase in bubble size is observed in the first 30 min, but this process stops afterwards. However, the suspension in this region is inhomogeneous which is due to the formation of large particle agglomerates at these higher surfactant concentrations. The formed agglomerates lead to formation of cracks during water drying and the final porous material is highly inhomogeneous, Fig. 4D.

Region 1UF (UF stands for "Unstable and Falls apart upon drying") is located at even higher surfactant concentrations $C_S/C_P \geqslant 0.06$ for 20 wt% particles. Wet foams in this region exhibited the same stability patterns as those in Region 1UC, except for the presence of more and bigger particle agglomerates. Because of these agglomerates, foams not only cracked but completely fell apart in the process of drying (Fig. 4E).

The comparison of these results with those for the surfactant adsorption on particle surface (Section 3.1) shows that the foams, formed from silica suspensions with low surface coverage (13–50 μg/m^2 CAPB), drained while those with higher surface coverage (e.g. 420 μg/m^2 CAPB) suffered from aggregation and cracked upon drying. Stable dry porous materials were obtained only with intermediate surface coverage of the silica particles, viz. around 110 μg/m^2 which corresponds to ≈20 times below the complete adsorption layer of surfactant on the silica surface.

Therefore, the observed four sub-regions are explained in the following way: in Region 1S, the surfactant components partially

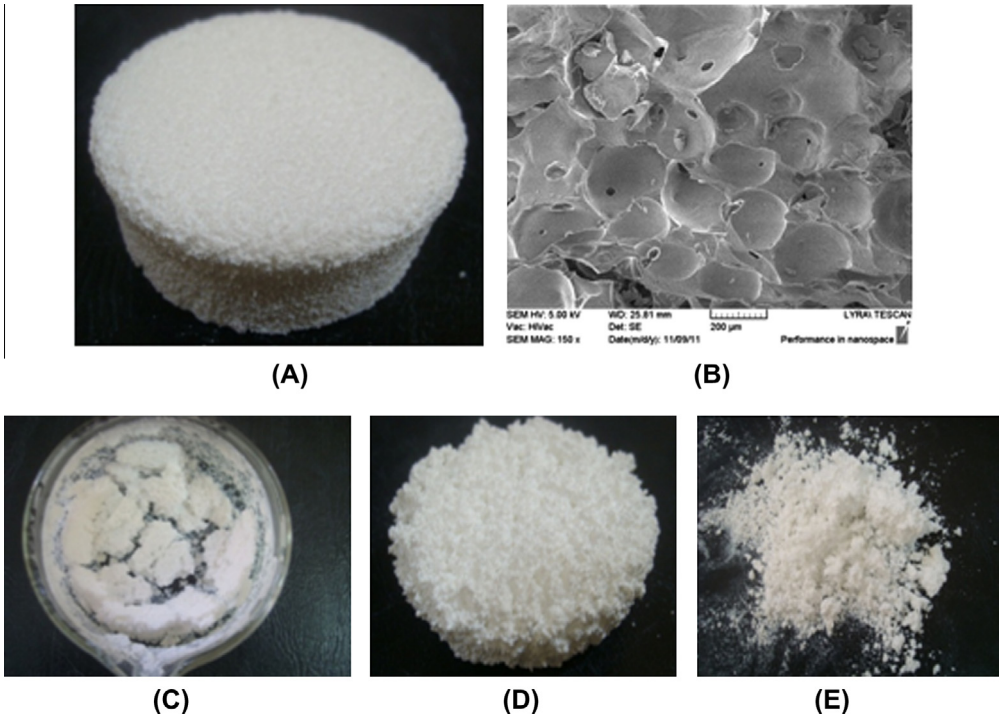

Fig. 4. Illustrative pictures of dried foams, generated from suspensions with compositions falling in (A) Region 1S; (C) Region 1UD; (D) Region 1UC and (E) Region 1UF. The SEM picture in (B) shows a dry foam from Region 1S.

hydrophobize the silica particles, so that the particles form a gelled network in the foamed suspension. This network is relatively strong and it prevents the liquid from drainage and the bubbles from Ostwald ripening. At lower surfactant concentrations, in Region 1UD, surfactant adsorption is insufficient to hydrophobize the particles and the latter remain too hydrophilic to form a strong network – as a consequence, bubble coarsening and water drainage is observed in this region. On the other side of Region 1S, in Region 1UC, the concentration of surfactant is sufficiently high to modify the particles and the latter attract each other very strongly – as a consequence, big particle agglomerates are formed and the suspension becomes inhomogeneous. These agglomerates lead to formation of cracks upon drying. The latter process is further enhanced in Region 1UF, where the interactions between the particles are very strong and very big agglomerates are formed. At even higher surfactant concentrations, in Region 2, the particle–particle attraction becomes so strong that the initial viscosity of the suspension is too high to allow efficient air entrapment in the used foaming device.

The following sections contain further experimental data and deeper discussion which support the mechanistic explanations described in the preceding paragraph.

3.4. Viscosity of CAPB-silica suspensions

The suspension viscosity may play an important role in the foaming process [19,22,23,41]. In most of the previous studies, the viscosity of the foamed suspensions was measured at shear rates which were not necessarily representative for the actual foaming conditions. This is probably the main reason for the different conclusions about the effect of suspension viscosity, reported in the various studies [19,22,41].

To characterize the viscosity of our suspensions under conditions, representing closely those in the actual foaming experiments, we used the procedure described in Section 2.4. The first important feature of this procedure is that the viscosity of the CAPB-silica suspension was measured at shear rates similar to those during foaming, as estimated from the model for the flow dynamics in the used planetary mixer. The second important feature of the procedure is that the viscosity was measured as a function of time, after mixing the particles and surfactant – in this way, we could determine how the suspension viscosity evolved in the course of the foaming process.

The results for the time dependence of the viscosity for suspensions containing 15.8 wt% particles, at different surfactant concentrations (expressed as C_S/C_P), are shown in Fig. 5A. For comparison, the viscosity of the silica suspension without CAPB was ≈4 mPa s – this suspension behaved as Newtonian fluid and its viscosity did not depend on time and on shear rate. The viscosity of the suspension with $C_S/C_P = 0.009$ (falling in Region 1UD, see Fig. 2B) was significantly higher, $\eta_{APP} \approx 12$ mPa s. Note that the foam prepared from this suspension had very high air volume fraction of 95 vol%, whereas no foam was formed from the silica suspension without any added surfactant. This significant difference in the foamability of these two suspensions, both with relatively low viscosity, is related to the fact that the silica particles are too hydrophilic to stabilize the air bubbles during foaming, whereas the addition of surfactant with concentration above its critical micelles concentration (CMC ≈ 0.031 wt% [40]) leads to stabilization of the trapped air bubbles by the surfactant – see Sections 3.6 and 4 below for further explanations on this point. The increased suspension viscosity in the presence of CAPB is due to the adsorption of some fraction of the surfactant on the silica surface, thus modifying the interactions between the dispersed silica particles. Nevertheless, the foams in Region 1UD were unstable with respect to liquid drainage, due to the relatively low yield stress of the respective suspensions, as explained in Section 3.5 below.

The suspensions in Region 1S had much higher apparent viscosity, between 100 and 250 mPa s, see the blue curves in Fig. 5. The viscosity of these suspensions did not change significantly during the first 600 s of shearing. Some increase of the apparent viscosity was observed afterwards. The latter effect was better seen at

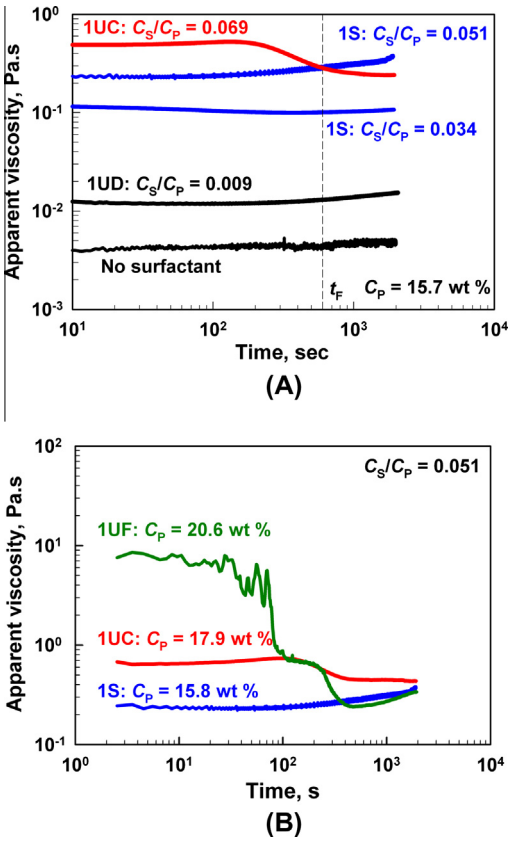

Fig. 5. Apparent viscosity as function of time for (A) C_P = 15.8 wt% silica at 100 s^{-1}, at different surfactant-to-particle ratios, C_S/C_P, and (B) C_S/C_P = 0.051 at different particle concentrations. The region, in which the respective foam falls (see Fig. 4), is indicated for each curve.

higher surfactant-to-particle ratios. This increase of viscosity is related to the formation of stronger network of attracting silica particles in the suspension which stabilizes the foam during shelf-storage and drying.

The suspensions having compositions in Region 1UC (crack formation upon drying) had noticeably different dependence $\eta(t)$, compared to those in Region 1S, see Fig. 5. For these suspensions, the initial viscosity was higher than the viscosity of the suspensions in Region 1S (in the first several minutes of shearing), but noticeably decreased afterwards – see the red[1] curves in Fig. 5. This decrease was accompanied with a formation of particle agglomerates in the silica suspension. These agglomerates were associated with the formation of cracks in the drying porous material.

Suspensions with composition corresponding to Region 1UF (e.g., C_S/C_P = 0.051 at C_P = 20.6 wt%) had shorter period, in which the viscosity remained constant, compared to Region 1UC. The initial viscosity of these suspensions was very high (above 7000 mPa s) and this viscosity rapidly decreased upon shearing, see the green curve in Fig. 5B. After 600 s, the viscosity of these suspensions was around 260 mPa s. This viscosity decrease was related to formation of big agglomerates in the suspension upon shearing. Similar agglomerates were observed in the foaming suspensions. The observed evolution of the suspension viscosity had obvious impact on the foamability of these suspensions – in the first 50 s, when the viscosity was above 5 Pa s, there was no air entrapment, see Fig. 1B. When the viscosity decreased, air entrapment was observed but the generated foams were unstable to drying.

The rheological properties of the samples, having compositions in Region 2 (low foaming) could not be characterized precisely by the rheological methods used here, because their apparent viscosity was above 10 Pa s immediately after loading the suspensions in the rheometer. This very high apparent viscosity of the suspensions was leading to suppressed air entrapment in the foaming experiments.

From all these experiments we can conclude that there is a correlation between the effective viscosity of the suspensions, their foaming properties, and the stability of the generated foams in the process of drying. A quantitative relation between the air volume fraction in the generated foams and the suspension viscosity is discussed in Section 4.1 below.

3.5. Suspension yield stress

The yield stress of the suspensions is another important characteristic which may affect the foam properties. Guignot et al. [42] showed that the increase of the suspension yield stress leads to a significant retardation of the liquid drainage from the foams. Guillermic et al. [43] showed that the addition of Laponite particles to SDS-stabilized foams also retards significantly the liquid drainage, however the authors observed that eventually, at longer times, the liquid drained from their foams.

As discussed in Section 3.3, we were able to suppress completely the liquid drainage from our foams, when appropriate surfactant and particle concentrations were used, see Fig. 4A. To check whether the boundary between the draining and non-draining foams is related to the suspension yield stress, we measured the rheological properties of the suspensions as described in Section 2.4. As expected, the studied suspensions had thixotropic behavior and their properties were different upon increase and decrease of the shear rate (see Fig. S3 in the supplementary materials). Because we are interested in the relation between the yield stress and the foam stability to drainage, in the further discussion we use the suspension yield stress while decreasing the shear rate, thus mimicking the processes occurring in the foams after stopping their shearing in the foaming device.

The rheological curves were fitted well by Bingham equation and the yield stress of the suspension was determined as a function of C_S/C_P, at C_P = 15.8, 17.9 and 20.6 wt%, see Fig. 6. One sees that the yield stress increases significantly with the increase of C_S/C_P from 0.01 to 0.03 for these particle concentrations. Further increase of C_S/C_P from 0.03 to 0.06 does not affect significantly the yield stress of the suspensions. The increase of particle concentration at given C_S/C_P also leads to increase of the suspension yield stress, as expected.

The analysis of all experimental data for the yield stress and for the liquid drainage from our foams, showed that the threshold yield stress of the suspension which arrested the foam drainage, was $\tau_0 \approx 10$ Pa – see the horizontal dashed line in Fig. 6. All foams with yield stress higher than 10 Pa were stable to drainage and vice versa. For explanation of this value and discussion of the involved mechanism of drainage arrest, see Section 4.2 below.

3.6. Optical observations of foams and foam films

Optical observations of foam films, formed from silica suspensions without CAPB, were performed by the procedure described in section 2.7. The typical evolution of these foam films for suspensions containing 15.8 wt% silica particles (no surfactant) is illustrated in Fig. 7A. One sees several consecutive stages in the process of film thinning: (1) many particle agglomerates are seen initially in the thick foam film, immediately after its formation.

[1] For interpretation of color in Fig. 5, the reader is referred to the web version of this article.

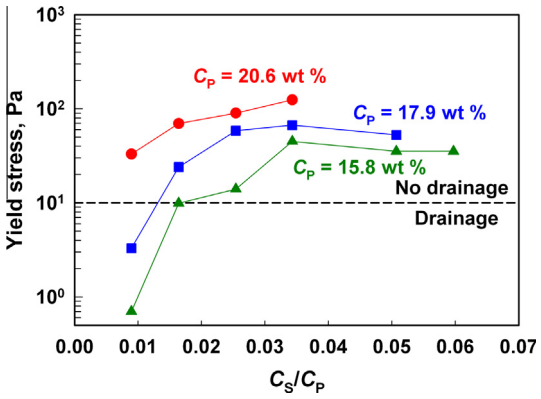

Fig. 6. Yield stress of the suspensions used for foaming, as a function of the surfactant-to-particle ratio, C_S/C_P, for suspensions containing 15.8 wt% (green triangles), 17.9 wt% (blue squares) and 20.3 wt% particles (red circles). Two different regions were observed with respect to foam drainage: the foams with yield stress below 10 Pa (the horizontal dashed line) were unstable to drainage, whereas all foams with yield stress above 10 Pa foams were stable to drainage. (For interpretation of the references to color in this figure legend, the reader is referred to the web version of this article.)

However, most of the silica particles leave the film for less than 10 s, when it becomes thinner than 100 nm. (2) During the further film thinning down to 80 nm, only several small particle aggregates remain visible inside the film – see the white spots in the picture, taken 30 s after film formation. (3) During the last stage of film thinning, virtually all silica particles left the foam film, the latter thinned down to 30 nm and ruptured. These observations show that the silica particles in the original aqueous suspensions are hydrophilic, do not adsorb on the air–water interface, and cannot stabilize the foam films. As a result, the silica suspensions without surfactant do not generate foam.

To study the effect of CAPB on foam film behavior, we observed foam films formed from CAPB-silica suspensions at the boundary between regions 1UD and 1S. The experiments with 15.8 wt% silica + 0.5 wt% CAPB dispersions showed that the behavior of the foam films depended significantly on the "pre-history" of the suspension, before film formation. When the film was formed around 10 min after mixing the particles with the surfactant solution, the film behaved as shown in Fig. 7B. Instead of film with circular periphery, a film with elliptic shape was usually formed. This film contained relatively small number of trapped particles and its thinning behavior was very similar to that observed for pure CAPB solution (except for the elliptic shape of the film periphery). This foam film was stable in a closed capillary cell, when the water evaporation from the film was suppressed. When we opened the experimental cell to the atmosphere and the water started to evaporate from the foam film, the particles in the meniscus region (around the film) became visible – see the last image in Fig. 7B. These particles obviously formed a network in the meniscus region around the foam film, which explains the non-circular shape of the films in these experiments – this non-circular shape is supported by the yield stress of the suspension and, therefore, did not relax to the typical circular shape of the foam films, corresponding to minimal area of the air–water interface. We conclude from these observations that the particles in the respective foams do not adsorb on the air–water interface, but form a 3-dimensional (3D) network around the bubbles, which suppresses the water drainage and decreases the rate of Ostwald ripening.

Our attempts to obtain foam films from suspensions in Regions 1UC, 1UF and 2 were unsuccessful, because these suspensions were too viscous and we could not control the liquid inside the capillary cell by the existing equipment.

To check whether the particles adsorb on the bubble surface and stabilize the foam films in Regions 1S and 2, we performed additional observations of actual foams, prepared in these regions as described in Section 2.3. We placed a foam in petri dish and observed in reflected light the foam films, formed between the uppermost layer of bubbles and the ambient atmosphere. Illustrative images from these observations are shown in Fig. S4 – one sees that the foam films appear dark and relatively homogeneous which is a clear indication that these films are stabilized by surfactant molecules, adsorbed on the film surfaces (not by trapped particles). Otherwise the films would appear bright and inhomogeneous when observed in reflected light.

From these experiments we conclude that the used silica particles, in the absence of surfactant, are too hydrophilic to stabilize the foam films and no foam is formed upon suspension agitation. When CAPB is added to the suspension, the foam films are stabilized by surfactant, while the particles form a 3D network in the neighboring Plateau borders and nodes of the foam.

4. Quantitative relations between the rheological and foaming properties of the suspensions

We can conclude from all results described in Section 3 that the optimal conditions for formation of stable foams correspond to particles which attract each other, due to hydrophobic forces, but still a significant electrostatic repulsion prevents the extensive

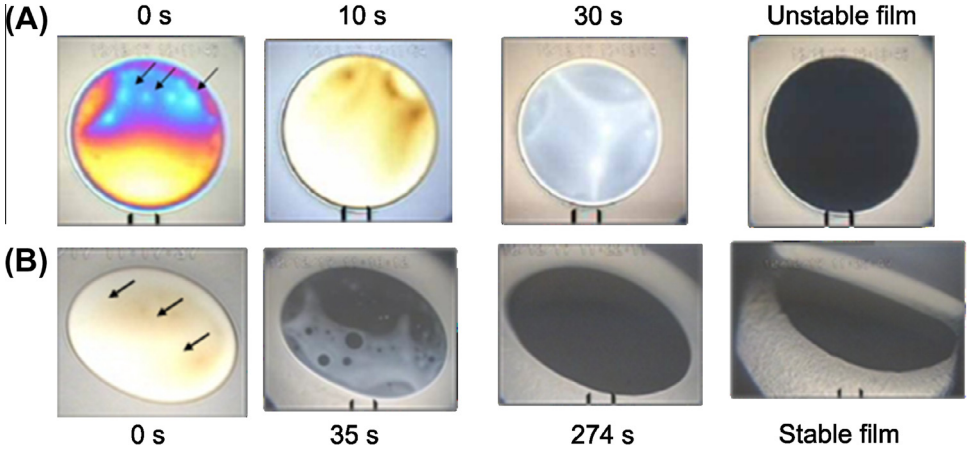

Fig. 7. Evolution of thinning foam films for systems containing 15.8 wt% silica: (A) without surfactant added, (B) with 0.5 wt% CAPB. The distance between the vertical dark marks at the bottom of these images is 50 μm.

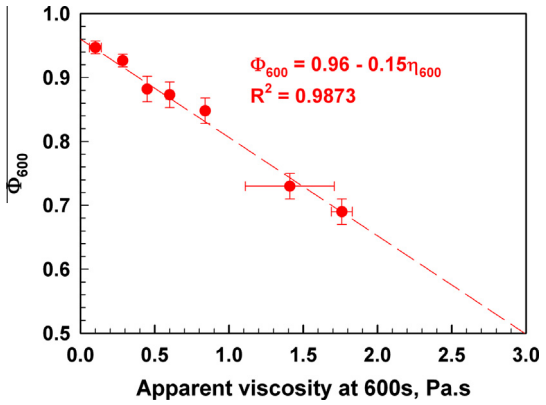

Fig. 8. Linear dependence of the air volume fraction after 600 s of foaming, Φ_{600s}, as a function of the apparent viscosity of the foamed suspension (measured 600 s after mixing the particle suspension with the CAPB solution).

particle agglomeration. These conditions favor the formation of a stable 3D-network within the silica suspension, possessing the desired optimal suspension viscosity and yield stress, which ensure both high foamability and high foam stability. Low surface coverage of the particles is sufficient to achieve the desired suspension properties, so that the formed foams can survive the water drainage and drying. Further surfactant adsorption leads to severe particle agglomeration in the suspension and to formation of cracks in the foam samples upon drying.

In the current section we compare the results from the foam tests (Figs. 1–4) with the results from the model experiments (Figs. 5–7) in order to quantify, whenever possible, the factors controlling the observed trends.

4.1. Dependence of the bubble volume fraction on suspension viscosity

As explained in Section 3, the different foamability of the suspensions containing CAPB and silica of various concentrations could be related to the different viscosities of these suspensions. To quantify this relation, we determined the suspension viscosity at appropriate shear rate and time after mixing of the surfactant and particles, in order to mimic closely the viscosity evolution in the actual foaming process. The characteristic foaming time was 600 s (see Fig. 1). Therefore, in Fig. 8 we plot the air volume fraction of the foam after 600 s, as a function of the suspension viscosity, η(600 s), determined as explained in Section 2.4. One sees that the experimental data fall around a single master line, described by a linear dependence:

$$\Phi_{600s} \approx 0.96 - 0.15\eta \quad (1)$$

where η is measured in Pa s and Φ_{600s} is dimensionless, varying between 0 and 1. The intercept of 0.96 corresponds to the air volume fraction of the foam formed from the studied CAPB solutions without added silica particles, i.e. with viscosity of ≈1 mPa s. The linear decrease of the air volume fraction with the increase of the apparent suspension viscosity is an empirical observation at the moment, which is worthy a further, more detailed investigation.

Note that we have excluded the data at 20.6 wt% particle concentration from this plot because the suspension viscosity decreased around 40 times within a short period of time during shearing of this sample, due to the extensive particle agglomeration (see Fig. 5B). Therefore, it was impossible to define unambiguously a viscosity value to be plotted in Fig. 8 for this system, because the time evolution in the rheometer and in the foaming device is not necessarily exactly the same, due to the different geometry of the sheared region.

Eq. (1) predicts (and our experiments confirm) that the volume fraction of the trapped air decreases below 35% when the viscosity of the suspension becomes higher than 4 Pa s. Therefore, the threshold viscosity for foam generation in the used foaming device is of the order of ca. 4 Pa s, which is in a reasonably good agreement with the results reported by Gonzenbach et al. [23] and Studart et al. [40]. This is an approximate estimate, because the exact dependence and limiting viscosity would certainly depend on the power and operational mode of the specific foaming device.

4.2. Relation between suspension yield stress, liquid drainage and bubble Ostwald ripening

After foaming, liquid drainage was observed from the foams generated in Region 1UD. Of particular interest for us is the transition between Regions 1UD and 1S, because only the foams in Region 1S are appropriate for production of dry porous materials. To the best of our knowledge, no quantitative relation has been proposed in the literature to describe the stability of foams to liquid drainage.

Several studies performed at low particle concentrations [7,12,13,16–18] showed that the increase of surfactant concentration up to a certain point led to slower drainage, with a characteristic drainage time of the order of hours. Several explanations were proposed in literature: increased viscosity of the suspension [16,17], drainage arrest [7], aggregation and modification of the surface charge and/or surface hydrophobicity of the particles [12,13]. Other studies showed that the enhanced stability to drainage of particle-stabilized foams is related to increased yield stress of the foamed suspension. Thus Dickinson et al. [6] suggested that stable foams could be produced at sufficiently high particle concentrations, when weak gels with thixotropic behavior and finite yield stress are formed. In the same line of consideration, Guillermic et al. [43] showed that the yield stress of Laponite-stabilized foams increased with suspension aging, which was related to enhanced foam stability to drainage. Guignot et al. [42] also showed that the increased yield stress could enhance particle retention in foams. All these studies were performed with foams which were unstable to drainage at long storage times – therefore, the rate of drainage was considered in these studies. In our notation, these foams are unstable and correspond to Region 1UD.

In contrast, Gonzenbach et al. [9,10] prepared foams with high concentrations of particles for which the liquid drainage was completely arrested. Vilkova et al. [14] also prepared stable foams in the presence of silica particles and showed that the foams in presence of about 40 mM hexylamine and 6 wt% silica did not drain and their suspensions had significantly higher yield stress (≈10 Pa) than that of the suspensions corresponding to draining foams (<1 Pa).

In our study we also found that all suspensions having a yield stress above 10 ± 1 Pa gave foams which were stable against drainage, see Fig. 6. To rationalize the latter value, we applied to the studied foams a model, proposed originally by Chaplain et al. [44] to describe the flow of a yield-stress fluid in a porous medium. According to this model, the flow of a yield-stress fluid in a porous medium is arrested when the fluid yield stress is higher than the driving flow pressure, at the scale of the pore structure. Considering the foam as a porous structure, and taking into account that the driving pressure for liquid drainage around the bubbles is the hydrostatic pressure, $\Delta\rho gd$, where $\Delta\rho$ is the mass density difference between bubbles and the surrounding suspension, g is gravity acceleration and d is the bubble diameter, one can estimate the threshold yield stress, above which the water drainage shall stop, as

$$\tau_{YD} \sim \Delta\rho gd \quad (2)$$

Applying this estimate to our foams, containing bubbles with mean diameter $d_{32} \approx 1$ mm, we estimate the threshold yield stress as $\tau_{YD} \approx 10$ Pa, which is in a very good agreement with the experimental results. Eq. (2) shows also that the threshold yield stress is proportional to the bubble size which explains why one observes a coupling between the Ostwald ripening (increasing the bubble size) and the liquid drainage from the foams, stabilized by particulate suspensions.

Furthermore, one could expect that the suspension yield stress could arrest the bubble Ostwald ripening in foams, when it becomes comparable to the driving force of the ripening, viz. to the difference between the capillary pressures of the bubbles. Taking into account that the this difference is of the order of $\Delta P_c \approx \sigma/R$ (where R is bubble radius), one estimates that the Ostwald ripening would stop when the yield stress or bubble size increase so that the balance

$$\tau_Y > \sigma/R \tag{3}$$

is satisfied. In our systems we observed usually that the initial bubbles with diameter of 100–200 μm were increasing their size, due to Ostwald ripening, until this size became of the order of 0.5–1 mm when the Ostwald ripening stopped for the foams in Regions 1S and 1UC. Introducing $\sigma \approx 0.03$ N/m and $R_{32} \approx 0.5$ mm we see that the yield stress should be of the order 60 Pa to arrest the Ostwald ripening. This value is rather reasonable keeping in mind that, as explained above, the process of suspension gelling (with the concomitant increase of the yield stress) continued after foam formation and could easily become higher than 50 Pa. The mechanistic explanation of the microscopic processes which realize the macroscopic balance in Eq. (3) will not be considered here – the reader could see the discussion in Section 3.2 of Ref. [36], and in the literature cited therein.

4.3. Relation between suspension aggregation and foam stability to drying

As explained in Section 3.3, particle agglomeration becomes very significant above certain concentrations of surfactant and the foams become unstable upon drying. Evidence for this extensive agglomeration is the observed decrease of the suspension viscosity with time, at constant shear rate (Fig. 5), and the large agglomerates seen in the structure of the dried foams (Fig. 4D and E).

The role of particle agglomeration could be illustrated convincingly by considering the viscosity of the suspensions after 600 s of mixing, as a function of surfactant-to particle ratio, see Fig. 9A. In these plots, the suspension viscosity increases almost linearly to a maximum and then decreased, for all particle concentrations of relevance. In agreement with the foaming and stability diagrams (Fig. 2) the viscosity increase was steeper at higher particle and surfactant concentrations. Comparison with the foam stability diagrams (Fig. 2B) showed that the maxima in these viscosity curves correspond to the transition from Region 1S, where the foams were stable to drying, to Region 1UC where extensive particle agglomeration and cracking of the drying foams were observed.

To confirm this relation between viscosity evolution and particle agglomeration, we prepared wetting layers from the suspensions in this transitional zone, around the maxima in the curves shown in Fig. 9A. These wetting films were prepared by spreading suspensions with a spatula on glass plates and were dried at ambient conditions. After drying, the deposited layers were observed in transmitted light (Fig. 9B and C). In agreement with the foam studies, the wetting layers at the maximum of viscosity, containing 15.8 wt% silica and $C_S/C_P = 0.041$ (Fig. 9B), were homogeneous and contained very low fraction of aggregates. Note that this suspension falls in region 1S. In contrast, the wetting layers of the suspension after the maximum, containing 20.4 wt% silica and $C_S/C_P = 0.035$ (Fig. 9C), contained many large aggregates in the range of 10–50 μm in diameter and the layer was cracked – this suspension falls in region 1UF, where cracking was also observed in the drying foams.

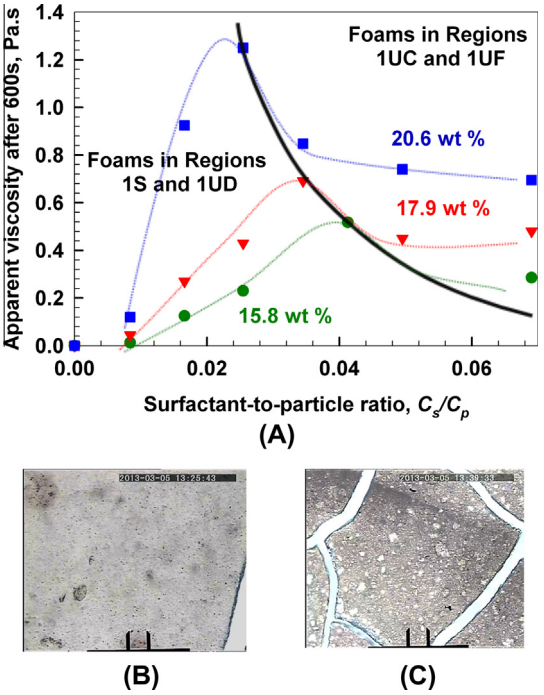

Fig. 9. (A) Apparent suspension viscosity after 600 s of mixing the silica suspension with the CAPB solution, as a function of surfactant-to-particle ratio for different particle concentrations. Dotted lines are guides to the eye and the solid line represents the transition between the region of stable foams and the region of unstable to drying foams. Dried spread layer of suspension containing (B) 15.8 wt% silica and $C_S/C_P = 0.041$ in Region 1S, and (C) 20.4 wt% silica and $C_S/C_P = 0.035$ in Region 1UC.

A mechanistic explanation of the relation between particle aggregation and foam cracking in the process of drying could be given, by considering the physical regimes of drying of porous materials [45]. This cracking is induced by capillary forces which develop differently in homogeneous and non-homogeneous drying samples. Briefly, the capillary forces in porous systems are directed towards regions containing pores with smaller size, because the larger pores release earlier their liquid water. For our systems this means that the capillary forces are directed predominantly from the periphery towards the more compact centers of the particle agglomerates in the suspensions. As a result, strong compression capillary forces appear in the non-homogeneous samples, which

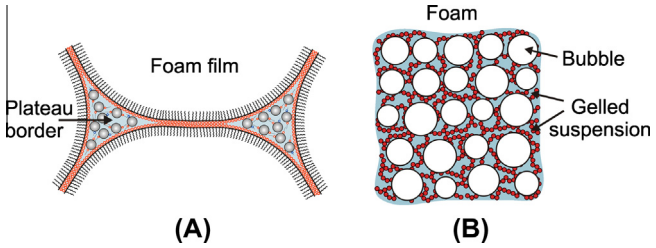

Fig. 10. Schematic presentation of the main mechanisms of foam stabilization in the silica + CAPB systems studied: (A) the foam films are stabilized against coalescence by adsorbed surfactant molecules; (B) gelled 3D-network of silica particles in the Plateau borders and nodes creates a yield stress and thus stabilizes the foam with respect to water drainage and bubble Ostwald ripening.

are directed to compact the big agglomerates present in these samples. Thus, each big agglomerate shrinks towards its center and gets separated from the neighboring agglomerates, which eventually leads to loss of mechanical integrity of the porous structure and even to complete disintegration of the drying porous structures (see Fig. 4D and E). In more homogeneous samples the pores have similar size and, therefore, the capillary stresses are more evenly distributed throughout the porous structure. As a result, the shrinking of the structure is affine and the structure integrity is not lost during drying. The quantitative analysis of these processes is beyond the scope of the present paper and it is postponed for a subsequent study.

5. Conclusions

In this paper we used a series of silica suspensions to clarify the main factors controlling the foamability and foam stability of concentrated particle suspensions, in the context of foams as precursors of porous materials. The main results and conclusions could be summarized as follows:

In the absence of CAPB, the original hydrophilic silica particles do not adsorb on the bubble surfaces, the foam films are unstable, the bubbles coalesce during foaming, and no foam is produced in the foaming device.

With the mixed silica + CAPB suspensions, two regions are observed with respect to suspension foaminess (see Fig. 2A): Region 1 – good foaming with air volume fraction higher than 35%, Region 2 – strongly reduced foaming. The transition between these two regions is entirely controlled by the suspension viscosity during foaming. The air volume fraction of the foams, generated after 600 s of stirring of suspensions falling in Region 1, decreases linearly with the increase of suspension viscosity, see Eq. (1).

With respect to foam stability, four sub-regions are observed in Region 1 (see Fig. 2B): Region 1S – stable foams which can be used for production of intact porous materials after drying; Region 1UD – unstable foam to water drainage; Region 1UC – stable foams to water drainage but unstable upon drying, due to crack formation inside the samples; Region 1UF – stable wet foams which fall apart upon drying. The foam films in all foams are stabilized by CAPB molecules, adsorbing on the bubble surface (see Fig. 10).

These regions are explained as follows:

In Region 1UD, the particle hydrophobization is insufficient to induce strong particle–particle attraction and to create a sufficient τ_Y of the silica suspension. As a result, these suspensions have $\tau_Y < 10$ Pa and liquid drainage is observed from the respective foams.

In Region 1S, the silica particles are sufficiently hydrophobized to increase the suspension $\tau_Y > 10$ Pa. As a result, CAPB molecules stabilize the bubbles against coalescence, while the gelled silica particles stabilize the foams with respect to liquid drainage and bubble Ostwald ripening. The stability of the foams to drainage is governed by Eq. (2). The particles attract each other in this region, however, they are homogeneously distributed in the suspension, without extensive particle agglomeration.

In region 1UC and 1UF the attraction between particles is too strong and the particles agglomerate extensively. As a consequence, the produced foams are inhomogeneous and become unstable upon drying.

Only the foams generated in Region 1S can be used to produce intact dry porous materials. These materials have two characteristic pore size ranges – one inherited from the size of the foam bubbles (200–300 μm in diameter) and another one reflecting the pore size distribution between the silica particles in the aggregates and agglomerates (in the nanometer range). These porous materials could be further modified by sintering, chemical or physical hydrophobization, impregnation with reactive solutions, or other procedures leading to new or improved functionality of the materials.

The reported concentration ranges for the particles and surfactant could be rather system specific and could depend strongly on particle shape and size, and on surfactant and particle charges. However, we expect that the observed effects of suspension viscosity, yield stress and particle agglomeration, discussed in Section 4, are of general relevance to this type of systems, as they reflect physical relations which are not system specific. Further quantitative studies with different particles and surfactants are needed to verify the range of systems which could be described by the proposed relations.

Acknowledgments

The authors gratefully acknowledge the help of several students and colleagues in the performed study: Monika Kovadjieva (foaming experiments), Radka Petkova (foam film observations), Borislava Damianova (HPLC measurements), Dr. Konstantin Golemanov (helpful discussions), all from Sofia University. The authors are grateful to Saint Gobain Recherche (SGR, Aubervilliers, France) for the support of this study and to the colleagues from SGR for the many useful discussions: Dr. Mathieu Joanicot, Dr. Marie Lamblet, Dr. David Louapre, Dr. Tamar Saison, and Dr. Valerie Goletto. The performed work is in the area of the European COST network MP1106 "Smart and green interfaces" and the project "Beyond Everest" of the Faculty of Chemistry & Pharmacy of Sofia University.

Appendix A. Supplementary material

Supplementary data associated with this article can be found, in the online version, at http://dx.doi.org/10.1016/j.jcis.2014.03.067.

References

[1] R.G. Alargova, D.S. Warhadpande, V.N. Paunov, O.D. Velev, Langmuir 20 (2004) 10371–10374.
[2] L.R. Arriaga, W. Drenckhan, A. Salonen, J. Rodrigues, R. Íñiguez-Palomares, E. Rio, D. Langevin, Soft Matter 8 (2012) 11085–11097.
[3] B.P. Binks, M. Kirkland, J.A. Rodrigues, Soft Matter 4 (2008) 2373–2382.
[4] B.P. Binks, T.S. Horozov, Angew. Chem., Int. Ed. 44 (2005) 3722–3725.
[5] B.P. Binks, R. Murakami, Nat. Mater. 5 (2006) 865–869.
[6] E. Dickinson, R. Ettelaie, T. Kostakis, B.S. Murray, Langmuir 20 (2004) 8517–8525.
[7] X. Dong, J. Xu, C. Cao, D. Sun, X. Jiang, Colloids Surf., A 353 (2010) 181–188.
[8] Z. Du, M.P. Bilbao-Montoya, B.P. Binks, E. Dickenson, R. Ettelaie, B.S. Murray, Langmuir 19 (2003) 3106–3108.
[9] U.T. Gonzenbach, A.R. Studart, E. Tervoort, L.J. Gauckler, Angew. Chem., Int. Ed. 45 (2006) 3526–3530.
[10] U.T. Gonzenbach, A.R. Studart, E. Tervoort, L.J. Gauckler, Langmuir 22 (2006) 10983–10988.
[11] G. Kaptay, Colloids Surf., A 230 (2003) 67–80.
[12] Q. Liu, S. Zhang, D. Sun, J. Xu, Colloids Surf., A 338 (2009) 40–46.
[13] Q. Liu, S. Zhang, D. Sun, J. Xu, Colloids Surf., A 355 (2010) 151–157.
[14] N.G. Vilkova, S.I. Elaneva, P.M. Kruglyakov, O.V. Dorchina, Reg. Architecture Eng. (in Russian) 2 (9) (2010) 20–30.
[15] W. Wang, B. Gu, L. Liang, W.A. Hamilton, J. Phys. Chem. B 108 (2004) 17477–17483.
[16] S. Zhang, Q. Lan, Q. Liu, J. Xu, D. Sun, Colloids Surf., A 317 (2008) 406–413.
[17] S. Zhang, D. Sun, X. Dong, C. Li, J. Xu, Colloids Surf., A 324 (2008) 1–8.
[18] S. Mishra, R. Mitra, M. Vijayakumar, Mater. Lett. 63 (2009) 2649–2651.
[19] P. Sepulveda, J.G. Binner, J. Eur. Ceram. Soc. 19 (1999) 2059–2066.
[20] C. Chuanuwatanakul, C. Tallon, D.E. Dunstan, G.V. Franks, Soft Matter 7 (2011) 11464–11474.
[21] P. Colombo, Philos. Trans. R. Soc., A 364 (2006) 109–124.
[22] S. Dhara, P. Bhargava, Int. J. Appl. Ceram. Technol. 3 (2006) 382–392.
[23] U.T. Gonzenbach, A.R. Studart, E. Tervoort, L.J. Gauckler, Langmuir 23 (2007) 1025–1032.
[24] I. Lesov, S. Tcholakova, N. Denkov, RSC Adv. 4 (2014) 811–823.
[25] A.R. Studart, U.T. Gonzenbach, I. Akartuna, E. Tervoort, L.J. Gauckler, J. Mater. Chem. 17 (2007) 3283–3289.
[26] G. Kaptay, Colloids Surf., A 282 (2006) 387–401.

[27] R.J.G. Lopetinsky, J.H. Masliyah, Z. Xu, Solid-stabilized emulsions: a review, in: B.P. Binks, T.S. Horozov (Eds.), Colloidal Particles at Liquid Interfaces, Cambridge University Press, Cambridge, 2006, pp. 186–224.
[28] K.P. Velikov, O.D. Velev, Novel materials derived from particles assembled on liquid surfaces, in: B.P. Binks, T.S. Horozov (Eds.), Colloidal Particles at Liquid Interfaces, Cambridge University Press, Cambridge, 2006, pp. 225–297.
[29] R. Aveyard, B.P. Binks, J.H. Clint, Adv. Colloid Interface Sci. 503 (2003) 100–102.
[30] B.P. Binks, Curr. Opin. Colloid Interface Sci. 7 (2002) 21–41.
[31] E. Dickinson, Interfacial particles in food emulsions and foams, in: B.P. Binks, T.S. Horozov (Eds.), Colloidal Particles at Liquid Interfaces, Cambridge University Press, Cambridge, 2006, pp. 298–327.
[32] S. Tcholakova, N. Denkov, A. Lips, Phys. Chem. Chem. Phys. 10 (2008) 1608–1627.
[33] B.P. Binks, T.S. Horozov, Colloidal particles at liquid interfaces: an introduction, in: B.P. Binks, T.S. Horozov (Eds.), Colloidal Particles at Liquid Interfaces, Cambridge University Press, Cambridge, 2006, pp. 1–76.
[34] B.P. Binks, J.A. Rodrigues, Angew. Chem., Int. Ed. 44 (2005) 441–444.
[35] N. Denkov, I.B. Ivanov, P. Kralchevsky, D.T. Wasan, J. Colloid Interface Sci. 150 (1992) 589–593.
[36] G.G. Fuller, E.J. Stancik, S. Melle, Particle-laden interfaces: rheology, coalescence, adhesion and buckling, in: B.P. Binks, T.S. Horozov (Eds.), Colloidal Particles at Liquid Interfaces, Cambridge University Press, Cambridge, 2006, pp. 169–187.
[37] S.S. Tzocheva, P.A. Kralchevsky, K.D. Danov, G.S. Georgieva, A.J. Post, K.P. Ananthapadmanabhan, J. Colloid Interface Sci. 369 (2012) 274–286.
[38] A.K.S. Chesterton, G.D. Moggridge, P.A. Sadd, D.I. Wilson, J. Food Eng. 105 (2011) 343–350.
[39] A. Scheludko, Adv. Colloid Interface Sci. 1 (1967) 391–464.
[40] A.R. Studart, R. Libanori, A. Moreno, U.T. Gonzenbach, E. Tervoort, L.J. Gauckler, Langmuir 27 (2011) 11835–11844.
[41] K.D. Danov, S.D. Kralchevska, P.A. Kralchevsky, K.P. Ananthapadmanabhan, A. Lips, Langmuir 20 (2004) 5445–5453.
[42] S. Guignot, S. Faure, M. Vignes-Adler, O. Pitois, Chem. Eng. Sci. 65 (2010) 2579–2585.
[43] R.M. Guillermic, A. Salonen, J. Emile, A. Saint-Jalmes, Soft Matter 5 (2009) 4975–4982.
[44] V. Chaplain, P. Mills, G. Guiffant, P. Cerasi, J. Phis. II 2 (2) (1992) 2145–2158.
[45] P. Coussot, Eur. Phys. J. B 15 (2000) 557–566.